Distribution and degradation trend of micropollutants in a surface flow treatment wetland revealed by 3D numerical modelling combined with LC-MS/MS

Loïc Maurer, Claire Villette, Nicolas Reiminger, Xavier Jurado, Julien Laurent, Maximilien Nuel, Robert Mose, Adrien Wanko, Dimitri Heintz

Distribution and degradation trend of micropollutants in a surface flow treatment wetland revealed by 3D numerical modelling combined with LC-MS/MS

Loïc Maurer[a,b], Claire Villette[a], Nicolas Reiminger[b,c] , Xavier Jurado[b,c], Julien Laurent[b] , Maximilien Nuel[b], Robert Mosé[b], Adrien Wanko[b], Dimitri Heintz[a]

[a]Plant Imaging and Mass Spectrometry (PIMS), Institut de biologie moléculaire des plantes, CNRS, Université de Strasbourg, 12 rue du Général Zimmer, 67084 Strasbourg, France.

[b]Département mécanique, ICube Laboratoire des sciences de l'ingénieur, de l'informatique et de l'imagerie, UNISTRA/CNRS/ENGEES/INSA, 2 rue Boussingault, 67000 Strasbourg, France.

[c]AIR&D, 67000, Strasbourg, France

Corresponding author

Dimitri Heintz

dimitri.heintz@ibmp-cnrs.unistra.fr

Abstract

Conventional wastewater treatment plants are not designed to treat micropollutants; thus, for 20 years, several complementary treatment systems, such as surface flow wetlands have been used to address this issue. Previous studies demonstrate that higher residence time and low global velocities promote nutrient removal rates or micropollutant photodegradation. Nevertheless, these studies were restricted to the system limits (inlet/outlet). Therefore, detailed knowledge of water flow is crucial for identifying areas that promote degradation and optimise surface flow wetlands. The present study combines 3D water flow numerical modelling and liquid chromatography coupled with high-resolution mass spectrometry (LC-HRMS/MS). Using this numerical model, validated by tracer experimental data, several velocity areas were distinguished in the wetland. Four areas were selected to investigate the waterflow influence and led to the following results: on the one hand, the number and concentration of micropollutants are independent of the waterflow, which could be due to several assumptions, such as the chronic exposure associated with a low Reynolds number; on the other hand, the potential degradation products (metabolites) were also assessed in the sludge to investigate the micropollutant biodegradation processes occurring in the wetland; micropollutant metabolites or degradation products were detected in higher proportions (both number and concentration) in lower flow rate areas. The relation to higher levels of plant and microorganism metabolites suggests higher biological activity that promotes degradation.

Keywords

Micropollutants, mass spectrometry, Computational Fluid Dynamics, water flow modelling, sludge, surface flow wetland.

1. Introduction

In the past decades, water quality and micropollutant issues have become major concerns in the water treatment field. Recent progress has confirmed this trend with the establishment of the Watch list in European laws (Decision 2015/495/EU of 20 March 2015) (Barbosa et al., 2016; Mailler et al., 2017). Micropollutants found in the environment have several origins, but urban wastewater is one of the most cited (Kasprzyk-Hordern et al., 2009; Luo et al., 2014; Petrie et al., 2015; Phillips et al., 2012; Verlicchi et al., 2012). Indeed, a wide variety of our daily activities generate micropollutants, which end up in wastewater (washing, cooking, or drug consumption) and, subsequently, in wastewater treatment plants (WWTPs). These wastewater treatment systems have not been designed to treat micropollutants. Nevertheless, in the literature, waste water treatment systems and, particularly constructed wetlands (CW), show their efficiency in the treatment of some micropollutants (Hijosa-Valsero et al., 2010; Matamoros and Bayona, 2006; Vymazal et al., 2017). In this way, part of the micropollutants can be caught by the different compartments of these systems, whereas others are released into the environment. Additionally, WWTPs face sustainability issues (reuse of water-derived resources and reduction of their environmental footprint) (Wang et al., 2015). Therefore, constructed wetlands and natural-based treatment systems seem to be well-suited to these new challenges. In Europe, complementary treatment systems have been installed for 20 years and can improve micropollutant removal and reduce the impact of direct release into the environment. WWTPs could disturb the environmental balance. For example, Tong et al. mention the impact of the nitrogen to phosphorus ratio

in lakes found near a WWTP outlet (Tong et al., 2020). Surface flow treatment wetlands (SFTW) are particularly popular in rural communities (Mara et al., 1992) and offer several benefits, such as complementary treatment for micropollutants—described in one of our previous studies (Nuel et al., 2018). Furthermore, the literature mentions hydraulics, specifically residence time, as one of the major factors that could influence micropollutant removal (Boonnorat et al., 2016; Ejhed et al., 2018; Esperanza et al., 2007; Gros et al., 2010). The increase in residence time can promote different mechanisms that are useful for micropollutant management. For example, longer residence time improves the biodegradation (Koch et al., 1999; Siegrist et al., 1995) of conventional pollutants, such as nutrients. Concerning micropollutants, photodegradation or sorption in sludge could be promoted by higher residence time in this kind of system (Rühmland et al., 2015), thus reducing their release into the environment. Nonetheless, most studies focus on the boundary conditions of the system (inlet/outlet) to characterise removal efficiency and compare global hydraulic parameters, such as residence time distribution. However, these global parameters could also hide the influence of specific areas inside water treatment systems. Therefore, a deep knowledge of hydraulics is crucial to understand the potential influence of water flow velocity on the distribution and degradation of micropollutants and would be useful to optimise the processes. Nonetheless, few studies consider different regions inside a system to compare those that could influence distribution or promote micropollutant removal (Gaullier et al., 2020). Among these studies, Mali et al. (2018) used a 2D hydrodynamics model combined with a passive scalar transport equation to determine metal distribution in a port. Their simulations show the influence of water flow velocity in the studied system. Another

study conducted by Gaullier et al. (2020) highlighted the heterogeneous distribution of pesticides in constructed wetlands using tracer experiments in different water flow velocity areas. Nevertheless, this study did not consider the degradation process, and therefore, the fate of these pesticides was not fully investigated. As such, the aim of this study was to obtain detailed knowledge of water flow velocities in a surface flow wetland and to determine if these velocities could influence micropollutant distribution and degradation. Therefore, we propose the first 3D surface wetland model based on real study site geometry combined with large-scale micropollutant screening. This transient water flow model was validated by a tracer experiment (comparison between experimental tracer experiment and simulation using a passive scalar transport equation) and built to define sludge collection areas. As sludge is a static compartment, micropollutants are sorbed according to their properties and affinity with solids and can provide a general overview of the chronic micropollutant load. In this way, micropollutant analysis was linked to water flow process modelling to understand the potential influence of the water flow velocity field on the spatial distribution and degradation of micropollutants.

2. Materials and methods

2.1. Study site

The study site is an SFTW located in Lutter (47°27’47.7″ N, 7°22’29.9″ E; Grand Est, France) and implemented in 2009. The SFTW is a shallow-water pond with an

68 impervious layer of clay to counter the high permeability of the natural soil. The SFTW
69 has a surface of 750 m², maximal width of approximately 13 m, maximal length of
70 approximately 40 m, and a heterogeneous depth. The SFTW has not yet been cleaned,
71 and mud has been accumulating since 2009. This SFTW was constructed at the outlet of a
72 two-stage vertical flow constructed wetland (VFCW) that collects wastewater (1000
73 population equivalent) before releasing it to the SFTW and, finally, into the river. All
74 details concerning SFTW can be found in Laurent et al. (2015).
75

76 ## 2.2. Hydrodynamics numerical model

77 ### 2.2.1. Water flow and passive scalar transport governing equations

78 Computational fluid dynamics (CFD) simulations were performed on OpenFOAM 4.0,
79 using the unsteady solver pimpleFoam, which was chosen for its ability to solve the
80 Navier–Stokes equations in unsteady mode and consider incompressible and turbulent
81 conditions for the flow resolution. Such turbulent conditions were observed in the SFTW
82 inlet. The corresponding continuity [1] and momentum equations [2] are given as:

83 $$\nabla . u = 0 \quad [1]$$

84 $$\frac{\partial u}{\partial t} + u\,\nabla u = -\nabla p + \upsilon \Delta u \quad [2]$$

85 where u is the velocity, p the pressure, υ the kinematic viscosity, and t the time. Because
86 of calculation costs constraints, only water flow was considered in this study. A tracker

simulation was performed to validate the model, considering the tracker as a passive scalar. The equation governing the passive scalar transport [3] is given as:

$$\frac{\partial C}{\partial t} + \nabla.(uC) - \nabla^2(D_m C) = q_m \quad [3]$$

where C is the tracker concentration, u is the velocity, t is the time, D_m is the tracker diffusion coefficient (sulforhodamine $D_m = 3.6\ 10^{-6}\ m^2.s^{-1}$), and q_m is the pollutant source term. A Reynolds-Averaged Navier-Stokes (RANS) method—with a turbulence closure scheme—was used to solve these equations. The standard k-Ɛ model was selected for the turbulence, as it is well-adapted for large flow fields and has been used in several water flow simulations in ponds (Alvarado et al., 2013; Ouedraogo et al., 2016). The simulations were performed using second-order schemes, and the results were extracted after convergence. All simulation results were obtained with residuals lower than 10^{-7}.

2.2.2. Computational domains and boundary conditions

The CFD model geometry was built using data collected in the field. Indeed, all the surface points defining the limits of the computational domain were obtained using a GPS system. The domain was then split into 1-square-meter subdomains, and the depth was measured manually using a bathymetry approach. All the data were used to build a 3D geometry of the SFTW. Figure S1 shows an overview of the study site used for the 3D model.

Regarding the boundary conditions, the following hypothesis was applied to the simulations. First, an inlet flow rate was defined for each simulation. SFTW flow rate

monitoring was performed using ultrasonic probes (IJINUS, MELLAC, France) and built-in exponential section venturis (ISMA, Forbach, France), as described by Nuel et al. (Nuel et al., 2017). Then, the average flow rate was calculated and used for each simulation. This hypothesis can be applied as the difference between the maximum and minimum SFTW flow rate measurements was not significant, according to the results obtained by Nuel et al. (Nuel et al., 2017). The outlet pressure was considered at the outlet, whereas no slip conditions were considered for the bank and the ground of the SFTW. Finally, symmetry conditions were used for the water surface. For the tracker experiment, an inlet mass flow rate was defined, with a mass flow rate of approximately 100 mg/s during the first 300 s of the simulation.

Subsequently, the geometry was meshed. The mesh size was chosen to fulfil a Y^+ criterion between 30 and 300 (in accordance with criteria for the standard k-Ɛ model), according to the recommendations found in Versteeg et al. (Versteeg and Malalasekera, 2007). This Y^+ criterion was calculated using Equation [4]:

$$\Delta s = \frac{\left(\frac{2}{0.026}\right)^{\frac{1}{2}} Y^+ \mu^{\frac{13}{14}}}{(\rho u)^{\frac{13}{14}} L^{-\frac{1}{14}}} \quad [4]$$

where u is the averaged velocity (m/s), ρ is the water density (kg.m^{-3}), μ is the dynamic viscosity (kg.m^{-1}.s^{-1}), L is the average water depth (m), and Δs is the mesh size in cm. Using this criterion, the recommended mesh size was between 1.1 and 11 cm. To reduce the calculation cost, the selected mesh size was 10 cm.

125 This choice was checked during the model validation step. The model resulting from
126 these choices has 1.5 million grid cells.

127 **2.2.3. Model validation**

128 The numerical model results were compared with the tracker experimental results
129 obtained in the field to ensure model and meshing validity. Tracer campaigns were
130 performed with sulforhodamine B (SRB, C27H29N2NaO7S2) as a fluorescent dye to
131 estimate the SFTW residence time, as described in detail in Laurent et al. (Laurent et al.,
132 2015). Briefly, an instantaneous pulse of tracer was injected at the inlet, and the tracer
133 concentrations were monitored by a fluorometer (GGUN-FL30, Albilia, Switzerland)
134 connected to a peristaltic pump operating continuously at 1 $L \cdot s^{-1}$. Fluorometer readings
135 were calibrated on site by water samples collected at the same location and spiked with
136 known tracer amounts.
137 These results were then compared to numerical simulations using the passive scalar
138 simulation described in Section 2.2.1. Alvarado et al. (Alvarado et al., 2013) and Coggins
139 et al. (Coggins et al., 2017) suggest the use of residence time to validate an SFTW water
140 flow model. Figure S2 underlines the proper fit between the simulated and experimental
141 curves. Thus, the model can reproduce the outlet signal. Based on the results, the model
142 was validated for the rest of the study.
143

144 **2.3. Chemicals**

145 Acetic acid and formic acid were acquired from Sigma Aldrich (St. Louis, MO, USA).
146 The extraction solvents (acetonitrile, methanol, and isopropanol) were obtained from
147 Fisher Chemicals (New Hampshire, USA). Ammonium formate was purchased from
148 Fluka Analytical (Missouri, USA), and NaOH was obtained from Agilent Technologies
149 (California, USA). Deionised water was obtained from a Direct-Q UV (Millipore) station.
150 Finally, the internal standards used, namely bezafibrate–d4, diclofenac-d4, gemfibrozil-
151 d6, N-desmethyl sildenafil-d8, sildenafil-d3, sulfamethoxazole-d4, were obtained from
152 Toronto Research Chemical (Ontario, Canada), whereas the acetaminophen-d4 standard
153 was purchased from Sigma Aldrich. The labelled internal standards were used to assess
154 the repeatability of the extraction process and to determine the limits of detection and
155 quantification (Villette et al., 2019a). The commercial standards used for compound
156 quantification (irbesartan, oxadiazon, tramadol, etofenprox, celiprolol, desvenlafaxine,
157 diflufenican, permethrin, propafenone, isoconazole, venlafaxine, fipronilulfone,
158 acebutolol, amiodarone, and climbazole) were purchased from Sigma Aldrich.

159

160

161 **2.5. Micropollutants extraction**

162 Micropollutants were analysed in the sludge samples. Water flow modelling defines the
163 sludge sampling strategy described in Section 3.1. In each defined area, a composite of
164 surface sludge (the first ten cm) was collected (in each season), as this layer was in direct
165 contact with the wastewater. The samples were stored at 4 °C before analysis. All

analyses were performed using 3 biological replicates. Micropollutants were extracted as described by Villette et al. (2019a). Briefly, 10 g of sludge was weighed, and double extraction was performed. The first overnight extraction was performed using 40 mL of acetonitrile:water (90:10) with 1% acetic acid at 4 °C under shaking with a magnetic stirrer. The samples were centrifuged for 15 min at 5500 rpm, and the supernatant was collected. Then, a second extraction was performed on the pellet using 20 mL of isopropanol:acetonitrile (90:10) for 15 min at 4 °C under shaking. The samples were centrifuged for 15 min at 5500 rpm, and the supernatant was recovered and freeze-dried. Finally, the samples were solubilised in 1 mL of acetonitrile:isopropanol:water (50:45:5). Parallel blank extraction was performed in each season.

2.6. Micropollutant analysis

The samples were analysed in liquid chromatography (LC) coupled to high-resolution mass spectrometry (HRMS). The method used (TargetScreener method (Bruker)) was mentioned in Villette et al., 2019a and Bergé et al., 2018. This method allows the targeted identification of drugs and pesticides but could also be investigated for non-targeted analysis. A DioneX Ultimate 3000 (Thermo) coupled to a Q-TOF Impact II (Bruker) was briefly used. The method was operated with two solvents: solvent A: H2O:MeOH (90:10 v:v) with 0.01% formic acid and 314 $mg.L^{-1}$ ammonium formate, and solvent B: MeOH with 0.01% formic acid and 314 $mg.L^{-1}$ ammonium formate. The compounds were separated using a C18 column (Acclaim TM RSLC 120 C18, 2.2 µm 120A 2.1x100 mm, Dionex bonded silica products) equipped with a C18 precolumn (Acquity UPLC ® C18, 1.7 µm, 2.1 × 5 mm). The compounds were analysed using the spectrometer in positive

188 ion mode with a spectra rate of 2 Hz, on a mass range from 30 to 1000 Da. Fragments
189 were obtained using broad-band collision-induced dissociation (bbCID) with an MS/MS
190 collision energy set at 30 eV. An analytical quality check was performed using a mix of
191 pesticides to assess the retention time (refs 31972 and 31978 Restek). The detailed
192 procedure and operational parameters can be found in Villette et al. 2019a.

193 **2.7. Data processing**

194 The annotations for the LC-HRMS/MS data were performed using TASQ 1.4 (Bruker
195 Daltonics), which contains a database of 2204 drugs and injected pesticides and has been
196 used to annotate ions in a targeted way based on the retention time, m/z value, isotopic
197 pattern of the parent ion (mSigma), and qualifier ions (daughter ion). Using this database,
198 which contains micropollutant commercial injection standards, all identification reached
199 level 1 according to the Schymanski classification. The selection criteria were a signal-to-
200 noise ratio higher than 3, a retention time variation lower than 0.3 min, an exact mass
201 variation lower than 3 ppm, and matching fragment ions when available. To obtain the
202 most representative view of the contamination, only micropollutants found in all seasons
203 and in 3 biological replicates with available commercial standards were quantified. The
204 mean concentration was determined using all the replicates, and the standard deviation
205 represents the variation found in the different seasons for each replicate.

206 Additionally, predicted catabolites and conjugates (metabolites) of the micropollutants
207 were annotated using in silico predictions performed in Metabolite Predict 2.0 (Bruker,
208 Germany) (Pelander et al., 2009). This annotation process has already been described in

209 Villette et al. (2019b). Briefly, 79 biotransformation rules were applied to the structure of
210 the parent drugs to generate metabolites over two generations. The software then
211 generated a list of raw formulae containing potential metabolites but also retrieved the
212 enzymes generating the metabolites. Finally, raw formula lists were imported into
213 Metaboscape 4.0. for annotation to perform suspect screening of the metabolites. The
214 data are compared with raw formulae generated using SmartFormula, as mentioned in
215 Villette et al., 2019b. The metabolites mentioned in this study were only those found in
216 all seasons and in 3 biological replicates.
217
218 Finally, the data were analysed using a non-targeted method following the processing
219 mentioned in Villette et al. (2019a). The annotations were performed using a criterion of
220 mass deviation lower than 3 ppm and mSigma value under 30 to assess the good fit of the
221 isotope pattern. Raw formula annotations were then generated using C, H, N, O, P, S, Cl,
222 I, Br, and F elements. Then, tentative identification (level 3 of the Schymanski
223 classification (Schymanski et al., 2015) was performed using analyte lists created from
224 the toxic exposome database (http://www.t3db.ca/), FooDB (http://foodb.ca/), EU
225 Reference Laboratories for Residues of Pesticides (http://www.eurl-pesticides.eu), Phenol
226 Explorer (http://phenol-explorer.eu/), Scientific Working Group for the Analysis of
227 Seized Drugs (http://www.swgdrug.org/), Norman Network (https://www.norman-
228 network.net/), PlantCyc (https://www.plantcyc.org/), KNapSAcK
229 (http://kanaya.naist.jp/KNApSAcK/), and SwissLipids (http://www.swisslipids.org/).
230 Additionally, the metabolites were analysed using a statistical enrichment approach that
231 is based on chemical similarity with the online ChemRICH tool

(http://chemrich.fiehnlab.ucdavis.edu/) (Barupal and Fiehn, 2017). All chemical identifiers (SMILES, PubChem ID, and InChIKey) were manually collected using the PubChem Identifier Exchanger tool (https://pubchem.ncbi.nlm.nih.gov/idexchange/idexchange.cgi). The identifiers were used to evaluate the structural similarity between the compounds based on chemical ontologies.

Additionally, the compounds were described using metabolic pathways; these networks were created using the MetaMapp online tool (http://metamapp.fiehnlab.ucdavis.edu/ocpu/library/MetaMapp2020/www/) (Barupal et al., 2012). The chemical identifiers were kept from ChemRICH analysis, and Kegg identifiers were manually searched in the Kegg database (https://www.genome.jp/kegg/), PubChem ID, SMILES, and MetaMapp. The Cytoscape 3.8.0 software was used to draw the different networks and biological pathways.

2.8. Statistical analysis

All samples were replicated three times. In a non-target way, each area was analysed separately; the samples were clustered in Metaboscape 4.0 (Bruker Daltonics) according to the seasons, and all the adduct forms were grouped in a bucket. Briefly, using the value count of group attributes, only compounds found in 80% of group samples (water flow areas) were selected. The metabolic profile was therefore investigated by comparing area by area based on a Wilcoxon rank sum test (non-parametric test). Results were considered significantly different using the fold change differences ≥ 2 or ≤ 2 and a *p-value* < 0.05. The fold change (associated with the different couples) and the associated

p-values were recovered for use in ChemRICH. The complete dataset (statistically differential and non-differential values) was submitted to ChemRICH, with the fold change converted to an average ratio. ChemRICH thresholds were *p-value* ≤ 0.05 and fold change ≥ 2 or ≤ -2 to consider that a compound is significantly up- or down-regulated in a specific condition (here, the pond) and to obtain the chemical enrichment analysis results.

3. Results

3.1. Water flow process modelling and areas selection

The SFTW was affected by weather conditions; thus, different inlet flow rates were measured. The distribution of these inlet flow rates measured during eight campaigns over a period of two years is shown in Figure S3.

Among these flow rates, one inlet flow rate condition per season (Figure 1) was simulated to underline the water flow velocity field diversity that could be observed on the SFTW. Simulations of the three slowest flow rates (winter with 7.2 $m^3.h^{-1}$, summer with 5.1 $m^3.h^{-1}$, and autumn with 4.2 $m^3.h^{-1}$) induced similar hydraulic behaviour, and a preferential flow between the inlet and outlet was observed. The increase in the inlet flow rate can generate vortices (simulation A in Figure 1), rendering the inlet-outlet link unclear. Nevertheless, Figure S3 highlights the extreme nature of this phenomenon.

276 Therefore, the spring simulation (simulation A in Figure 1) in which vortices appear, was
277 excluded from the rest of the study. The similar water flow behaviour observed in the
278 three other simulations provided a global overview of the SFTW hydraulic behaviour.
279 Even if a slow flow rate was created at the SFTW inlet, variations could be observed, and
280 the water flow velocity field seems to be particularly low near the banks in comparison to
281 other SFTW areas. Relatively higher water flow can be observed near the inlet and outlet,
282 whereas a low inlet flow rate is always detected in the SFTW; thus, areas were clustered
283 according to perpetual (inlet, outlet, and preferential flow areas) or rare (areas near the
284 banks) water flow.

285
286
287

288 According to the three lowest flow rate simulations (Figure 1), a sampling strategy was
289 defined to collect sludge samples in the different flow rate areas. Four areas were
290 selected, as depicted in Figure 2. The principal points of the water treatment system with
291 relatively higher and perpetual flows (the inlet (area a) and outlet (area d), respectively)
292 were selected. To overcome these boundary conditions, two areas were chosen
293 considering the water flow heterogeneity inside the SFTW. Therefore, sludge was
294 collected in an area with an intermediate higher and perpetual flow rate (defined in Figure
295 2 as area b) and in areas near the banks with very low flow rate (area c). These areas were
296 used for different seasonal sampling campaigns to analyse micropollutants and to
297 understand the influence of flow rate on the presence of micropollutants in the sludge.

3.2. Distribution of identified micropollutants according to the water flow areas.

Micropollutant analysis was performed for each season in the areas of interest; results are given in Figure S4 and Dataset 1. Micropollutant distributions fluctuate by season and are apparently unrelated to water flow.

To overcome the seasonal effect and obtain a global overview, only the compounds found in all seasons were considered; the results are shown in Figure 3. This general analysis indicates that the number of micropollutants found in the different sampling areas seems to be similar. Indeed, seven micropollutants were found in areas b and d, six in area c, and four in area a. Additionally, most of the compounds were found in at least two sampling areas, even if some micropollutants were only detected in a single area, and more than half of the micropollutants detected (100% in area a, 71% in area b and d, and 67% in area c) were found in at least two areas. Most micropollutants had concentrations between 40–400 $\mu g.kg^{-1}$ of sludge, and little variation in concentration was noticed between the different detection areas. For example, irbesartan was detected at concentrations between 76–125 $\mu g.kg^{-1}$. Only celiprolol was found at a higher concentration in area c (491 $\mu g.kg^{-1}$ in area a and 1187 $\mu g.kg^{-1}$ in area c).

3.3. Distribution of micropollutants metabolites in the different water flow areas

Studies show that the analysis of parent compounds alone underestimates the amounts of micropollutants found in the environment. Metabolites (potential conjugates or degradation products) could be found in higher quantities than parent compounds (Yin et al., 2017). Therefore, micropollutant metabolites (predicted derivatives) were also analysed for each season in the areas of interest; the results are shown in Figure S4 and Dataset 2. A similar trend can be found in the different seasons with a higher number of metabolites in relatively low water flow areas (b, c).

This general trend is highlighted by the compounds found in all seasons in Figure 4, and the global overview indicates that more compounds are identified in lower flow rate areas (14 in area b and 15 in area c) than in higher flow rate areas (4 in area a and 6 in area d). Additionally, very few compounds are common to different areas, and a wide variety of metabolite intensities were detected.

335

336
337

338 Several drugs and their metabolites were studied (Figure 5), and higher amounts of
339 tramadol and venlafaxine were found. Higher diversity in area c and irbesartan
340 metabolites in area b were detected, suggesting that the lower flow rate influences
341 metabolization. However, the number of metabolites detected is not necessarily related to
342 the amount of parent compounds; the number of metabolites is positively correlated for
343 tramadol (higher numbers of metabolites when tramadol is not detected), whereas the
344 opposite phenomenon was observed for venlafaxine (higher numbers of metabolites when
345 the venlafaxine concentration is approximately 123 $\mu g.kg^{-1}$ sludge).

346 **4. Discussion**

347 **4.1. Influence of boundary conditions**

348

349 Figures 1 and 2 highlight the low-velocity field in the SFTW, which could be caused by
350 several phenomena, such as the low inlet flow rates compared to the pond sizes, the head
351 losses resulting from the presence of vegetation, the shallow depth, and the rough sides.
352 The influence of water depth was investigated by Coggins et al., with a focus on the
353 impact of sludge accumulation on hydraulic performance (Coggins et al., 2017). Thus,
354 the areas of SFTW that contain the most accumulated sludge and the areas near the banks
355 have the lowest flow velocity field and are characterised by a very high hydraulic
356 residence time and, consequently, a low solid transport phenomenon. However, water

357 quality with higher nutrient removal (nitrogen and phosphorus) can be improved by
358 increasing residence time (Akratos and Tsihrintzis, 2007; Huang, 2000). A higher water
359 flow velocity field was detected at the boundary points of the system (inlet and outlet
360 area) due to the boundary conditions (constrictions), leading to a high rate of sludge
361 renewal.
362
363 **4.2. No correlation between parent compounds distribution and water flow**
364 **velocities**
365 The micropollutant analysis performed in different areas did not highlight significant
366 differences in their number and concentration, except for celiprolol. Indeed, almost the
367 same number of micropollutants and similar concentrations were found in these areas.
368 However, according to the literature, the sedimentation and sequestration of compounds
369 in the solid phase should be promoted in lower water flow velocity fields (Montiel-León
370 et al., 2019). These comments are supported by studies that have investigated the
371 influence of water flow velocities on contaminant concentrations and sequestration
372 (Gaullier et al., 2020; Mali et al., 2018). Gaullier et al. (2020) suggest that higher
373 pesticide storage in lower velocity areas is related to transport types (convection is
374 promoted in high velocity areas), and Mali et al. found higher metal deposition in a
375 weaker flow in a port (Mali et al., 2018); nevertheless, the higher velocities mentioned in
376 their study impact flow patterns and could partly explain the differences.
377 Therefore, our study used deep knowledge of water flow in treatment systems to
378 determine that water flow velocity fields are not the key parameters governing the
379 distribution of micropollutants. The difference in water velocities is unlikely to

significantly influence a specific micropollutant distribution. The Reynolds number in the SFTW was low, and the flow observed in the SFTW was generally laminar or low turbulent (except at the inlet and outlet), reducing the velocity difference in these areas. This trend was confirmed by the analysis of the areas of xenobiotics putatively identified in all the sampling areas shown in Figure S6. This broader view highlights that most of the micropollutants are found in similar proportions in different areas (fold change < 2 (absolute value)). Additionally, the study of physicochemical properties (log Kow, solubility, pka), as mentioned in Li et al. (2019), does not highlight any correlation between micropollutant detection and these properties.

The impact of water flow velocity could probably be highlighted by other assumptions, such as solid transport or higher inlet flow rate, probably helps distinguish areas based on their micropollutant composition. If velocity differences between SFTW areas are increased, sequestration could be affected. However, all the results found for these micropollutants should be tempered with the distribution of all the putative identifications from non-targeted analyses (Figure S7). The general trend emphasizes that the low flow rate area (area c) seems to accumulate slightly more xenobiotics and plant metabolites than other areas. These results are apparently more coherent with those found in the literature.

Another assumption that may explain the lack of differences (in concentration or area) could be related to parent compound degradation, as higher sedimentation probably occurs in the lower flow rate areas. However, this sedimentation should be hidden by degradation, which has also been enhanced in these areas.

4.3. *In situ* low water flow areas promote micropollutant degradation

Parent compounds have been found in minor amounts compared to their metabolites (Yin et al., 2017). This degradation process could not be neglected in the SFTW, as micropollutant biodegradation with conjugations and deconjugations has been described in this type of system (Tiwari et al., 2017). In our study, the distribution of micropollutant metabolites appears to be primarily influenced by water flow, and more biotransformation products are found in areas with scarce water flow (14 in area b and 15 in area c versus 4 and 6 in areas a and d, respectively). However, these areas are not located in the principal water flow channel and could be subject to intermittent flow. Rožman et al. highlight that a system with intermittent water flow provides a higher biodegradation capacity than one with permanent water flow, due to the biofilm development (Rožman et al., 2018). These conclusions support our observations. Additionally, areas with higher residence time can provide conditions stimulating degradation, such as increased potential contact time with microorganisms. The influence of prolonged contact time in a bioreactor to improve micropollutant transformation has been demonstrated (Asif et al., 2018; Boonnorat et al., 2016).

Similarly, the results shown in Figure 5 suggest that the higher numbers of micropollutant metabolites in the lower flow rate areas (b and c) is not necessarily related to the number of parent compounds, as phenomena, such as metabolite transport, could occur. A broader analysis of the data shows that the metabolite distribution apparently follows a general trend. A closer look at the elemental composition reveals that compounds with less than 15 or 10 carbons showed the same distribution as that described for

425 micropollutant metabolites (Figure S8 and dataset S3). The lower flow rate areas (b or c)
426 seem to stimulate compound deposition and transformation, and the conditions promoting
427 biodegradation were indicated by the non-target analysis and chemical class investigation
428 using ChemRICH (Barupal and Fiehn, 2017) (Figure S9). The results highlight the
429 specific detection of alkaloids and monoterpenes in the lower velocity areas; such
430 observations are not surprising, as plants grow near wetland banks. Additionally,
431 phosphatidylethanolamines, the primary component of the bacterial membrane, were also
432 detected. Therefore, the compound annotations seem to indicate higher biological
433 activities that combine plants and microorganisms. Furthermore, investigation of the
434 networks and biological pathways detected in the different areas (Figure S10) also
435 suggests a higher biological activity in lower velocity areas. Complex relationships were
436 primarily observed in the lower velocity areas (area c), and the network data showed that
437 succinate was mainly found in the low-flow-rate area. On the one hand, Nguyen et al.
438 demonstrated that bacteria fed with this succinate could improve energetic efficiency,
439 leading to a higher drug (sulfomethoxazole) removal rate (Nguyen et al., 2017). On the
440 other hand, this activity was also observed with the detection of p-cymene detection,
441 which is a biogas marker and component of anaerobic digestion. (Moreno et al., 2014)

442 Finally, a general biodegradation process seems to occur in SFTW. Most of the
443 metabolites found (59%) seem to be generated according to a biodegradation process
444 using cytochrome P450 hydroxylation or epoxidation followed by different transferase,
445 dehydrogenase, hydrolase, and esterase activities (Figure S11). Cytochrome P450 plays a
446 key role in Phase I metabolism for several herbicides, can degrade a wide variety of

447 micropollutants due to their low specificity (Cañameras et al., 2015), and could explain
448 the general process described here. This study was restricted to biodegradation, but other
449 abiotic processes, such as photodegradation or environmental conditions (pH, redox),
450 could also be considered to understand the fate of micropollutants in the SFTW (De
451 Laurentiis et al., 2012; Ávila et al., 2013; Lee et al., 2014; Rühmland et al., 2015).

452 **5. Conclusion**

453

454 This study investigated micropollutant distribution and degradation trends in SFTW
455 wetlands. The investigation was conducted by combining the following:

456 - a deep knowledge of hydraulic behaviour in the SFTW obtained through a 3D model
457 based on real study site geometry

458 - Large-scale screening of micropollutants and their metabolites

459 Based on this new approach, the results underlined the following micropollutant
460 behaviours in the SFTW wetland:

461 - A homogeneous distribution of parent compounds throughout the SFTW wetland
462 - Higher amounts of micropollutant metabolites in lower flow rate areas than in
463 areas with faster flow rates.

464 Therefore, the low flow rate conditions seem to promote degradation, and the results
465 suggest that:

466 - the velocity differences have an impact on metabolite distribution

- environmental conditions promoting micropollutant degradation are found in low flow rate conditions
- higher biological activity was detected due to the higher number of microorganisms or plant metabolites and the analysis of small molecules (molecular formula comprised of less than 15 or 10 carbons)

Future research needs should be considered to strengthen micropollutant distribution and degradation trends in water treatment systems. For example, the results obtained in this study highlighted the independence of micropollutant distribution from the velocity field but were obtained on our models that did not considered, for example, transport of solids or abiotic transformations. Therefore, these assumptions could be considered in future research. Additionally, the results were only obtained for SFTW wetlands. To strengthen the conclusions observed in this kind of system, the results should be compared with those of different systems operating in different geographical areas with different flow rates.

Acknowledgments

We acknowledge the Agence de l'Eau Rhin Meuse (AERM) and the village of Lutter for access to the SFTW.

Funding sources: This project was funded by a grant from the Agence de l'Eau Rhin Meuse (AERM) (grant number 183 696).

Author Contributions

Loïc Maurer performed the CFD modelling, sample preparation, data analysis, prepared the figure, designed the research, and wrote the manuscript. Claire Villette performed LC-Q-TOF-HRMS/MS data acquisition and discussed the manuscript. Nicolas Reiminger, Xavier Jurado, and Julien Laurent participated in the CFD modelling and discussed the manuscript. Adrien Wanko discussed the manuscript. Maximilien Nuel monitored the water flow on the study site. Robert Mosé discussed the manuscript. Dimitri Heintz discussed the manuscript and designed the research.

References

Akratos, C.S., Tsihrintzis, V.A., 2007. Effect of temperature, HRT, vegetation and porous media on removal efficiency of pilot-scale horizontal subsurface flow constructed wetlands. Ecological Engineering 29, 173–191. https://doi.org/10.1016/j.ecoleng.2006.06.013

Alvarado, A., Vesvikar, M., Cisneros, J.F., Maere, T., Goethals, P., Nopens, I., 2013. CFD study to determine the optimal configuration of aerators in a full-scale waste stabilization pond. Water Research 47, 4528–4537. https://doi.org/10.1016/j.watres.2013.05.016

Asif, M.B., Hai, F.I., Dhar, B.R., Ngo, H.H., Guo, W., Jegatheesan, V., Price, W.E., Nghiem, L.D., Yamamoto, K., 2018. Impact of simultaneous retention of micropollutants and laccase on micropollutant degradation in enzymatic membrane bioreactor. Bioresource Technology 267, 473–480. https://doi.org/10.1016/j.biortech.2018.07.066

Ávila, C., Reyes, C., Bayona, J.M., García, J., 2013. Emerging organic contaminant removal depending on primary treatment and operational strategy in horizontal subsurface flow

519 constructed wetlands: Influence of redox. Water Research 47, 315–325.
520 https://doi.org/10.1016/j.watres.2012.10.005
521 Barbosa, M.O., Moreira, N.F.F., Ribeiro, A.R., Pereira, M.F.R., Silva, A.M.T., 2016. Occurrence
522 and removal of organic micropollutants: An overview of the watch list of EU Decision
523 2015/495. Water Research 94, 257–279. https://doi.org/10.1016/j.watres.2016.02.047
524 Barupal, D.K., Fiehn, O., 2017. Chemical Similarity Enrichment Analysis (ChemRICH) as
525 alternative to biochemical pathway mapping for metabolomic datasets. Scientific Reports
526 7, 14567. https://doi.org/10.1038/s41598-017-15231-w
527 Barupal, D.K., Haldiya, P.K., Wohlgemuth, G., Kind, T., Kothari, S.L., Pinkerton, K.E., Fiehn,
528 O., 2012. MetaMapp: mapping and visualizing metabolomic data by integrating
529 information from biochemical pathways and chemical and mass spectral similarity. BMC
530 Bioinformatics 13, 99. https://doi.org/10.1186/1471-2105-13-99
531 Bergé, A., Buleté, A., Fildier, A., Mailler, R., Gasperi, J., Coquet, Y., Nauleau, F., Rocher, V.,
532 Vulliet, E., 2018. Non-target strategies by HRMS to evaluate fluidized micro-grain
533 activated carbon as a tertiary treatment of wastewater. Chemosphere 213, 587–595.
534 https://doi.org/10.1016/j.chemosphere.2018.09.101
535 Boonnorat, J., Techkarnjanaruk, S., Honda, R., Prachanurak, P., 2016. Effects of hydraulic
536 retention time and carbon to nitrogen ratio on micro-pollutant biodegradation in
537 membrane bioreactor for leachate treatment. Bioresource Technology 219, 53–63.
538 https://doi.org/10.1016/j.biortech.2016.07.094
539 Cañameras, N., Comas, J., Bayona, J.M., 2015. Bioavailability and Uptake of Organic
540 Micropollutants During Crop Irrigation with Reclaimed Wastewater: Introduction to
541 Current Issues and Research Needs, in: Fatta-Kassinos, D., Dionysiou, D.D., Kümmerer,
542 K. (Eds.), Wastewater Reuse and Current Challenges, The Handbook of Environmental
543 Chemistry. Springer International Publishing, Cham, pp. 81–104.
544 https://doi.org/10.1007/698_2015_412
545 Coggins, L.X., Ghisalberti, M., Ghadouani, A., 2017. Sludge accumulation and distribution
546 impact the hydraulic performance in waste stabilisation ponds. Water Research 110, 354–
547 365. https://doi.org/10.1016/j.watres.2016.11.031
548 De Laurentiis, E., Chiron, S., Kouras-Hadef, S., Richard, C., Minella, M., Maurino, V., Minero,
549 C., Vione, D., 2012. Photochemical Fate of Carbamazepine in Surface Freshwaters:
550 Laboratory Measures and Modeling. Environ. Sci. Technol. 46, 8164–8173.
551 https://doi.org/10.1021/es3015887
552 Ejhed, H., Fång, J., Hansen, K., Graae, L., Rahmberg, M., Magnér, J., Dorgeloh, E., Plaza, G.,
553 2018. The effect of hydraulic retention time in onsite wastewater treatment and removal
554 of pharmaceuticals, hormones and phenolic utility substances. Science of The Total
555 Environment 618, 250–261. https://doi.org/10.1016/j.scitotenv.2017.11.011
556 Esperanza, M., Suidan, M.T., Marfil-Vega, R., Gonzalez, C., Sorial, G.A., McCauley, P.,
557 Brenner, R., 2007. Fate of sex hormones in two pilot-scale municipal wastewater
558 treatment plants: Conventional treatment. Chemosphere 66, 1535–1544.
559 https://doi.org/10.1016/j.chemosphere.2006.08.020
560 Gaullier, C., Dousset, S., Baran, N., Kitzinger, G., Coureau, C., 2020. Influence of
561 hydrodynamics on the water pathway and spatial distribution of pesticide and metabolite
562 concentrations in constructed wetlands. Journal of Environmental Management 270,
563 110690. https://doi.org/10.1016/j.jenvman.2020.110690
564 Gros, M., Petrović, M., Ginebreda, A., Barceló, D., 2010. Removal of pharmaceuticals during
565 wastewater treatment and environmental risk assessment using hazard indexes.
566 Environment International 36, 15–26. https://doi.org/10.1016/j.envint.2009.09.002

Hijosa-Valsero, M., Matamoros, V., Martín-Villacorta, J., Bécares, E., Bayona, J.M., 2010. Assessment of full-scale natural systems for the removal of PPCPs from wastewater in small communities. Water Research 44, 1429–1439. https://doi.org/10.1016/j.watres.2009.10.032

Huang, J., 2000. Nitrogen removal in constructed wetlands employed to treat domestic wastewater. Water Research 34, 2582–2588. https://doi.org/10.1016/S0043-1354(00)00018-X

Kasprzyk-Hordern, B., Dinsdale, R.M., Guwy, A.J., 2009. The removal of pharmaceuticals, personal care products, endocrine disruptors and illicit drugs during wastewater treatment and its impact on the quality of receiving waters. Water Research 43, 363–380. https://doi.org/10.1016/j.watres.2008.10.047

Koch, G., Pianta, R., Krebs, P., Siegrist, H., 1999. Potential of denitrification and solids removal in the rectangular clarifier. Water Research 33, 309–318. https://doi.org/10.1016/S0043-1354(98)00220-6

Laurent, J., Bois, P., Nuel, M., Wanko, A., 2015. Systemic models of full-scale Surface Flow Treatment Wetlands: Determination by application of fluorescent tracers. Chemical Engineering Journal 264, 389–398. https://doi.org/10.1016/j.cej.2014.11.073

Lee, E., Shon, H.K., Cho, J., 2014. Role of wetland organic matters as photosensitizer for degradation of micropollutants and metabolites. Journal of Hazardous Materials 276, 1–9. https://doi.org/10.1016/j.jhazmat.2014.05.001

Li, Y., Sallach, J.B., Zhang, W., Boyd, S.A., Li, H., 2019. Insight into the distribution of pharmaceuticals in soil-water-plant systems. Water Research 152, 38–46. https://doi.org/10.1016/j.watres.2018.12.039

Luo, Y., Guo, W., Ngo, H.H., Nghiem, L.D., Hai, F.I., Zhang, J., Liang, S., Wang, X.C., 2014. A review on the occurrence of micropollutants in the aquatic environment and their fate and removal during wastewater treatment. Science of The Total Environment 473–474, 619–641. https://doi.org/10.1016/j.scitotenv.2013.12.065

Mailler, R., Gasperi, J., Patureau, D., Vulliet, E., Delgenes, N., Danel, A., Deshayes, S., Eudes, V., Guerin, S., Moilleron, R., Chebbo, G., Rocher, V., 2017. Fate of emerging and priority micropollutants during the sewage sludge treatment: Case study of Paris conurbation. Part 1: Contamination of the different types of sewage sludge. Waste Management 59, 379–393. https://doi.org/10.1016/j.wasman.2016.11.010

Mali, M., Malcangio, D., Dell' Anna, M.M., Damiani, L., Mastrorilli, P., 2018. Influence of hydrodynamic features in the transport and fate of hazard contaminants within touristic ports. Case study: Torre a Mare (Italy). Heliyon 4, e00494. https://doi.org/10.1016/j.heliyon.2017.e00494

Mara, D.D., Mills, S.W., Pearson, H.W., Alabaster, G.P., 1992. Waste Stabilization Ponds: A Viable Alternative for Small Community Treatment Systems. Water and Environment Journal 6, 72–78. https://doi.org/10.1111/j.1747-6593.1992.tb00740.x

Matamoros, V., Bayona, J.M., 2006. Elimination of Pharmaceuticals and Personal Care Products in Subsurface Flow Constructed Wetlands. Environmental Science & Technology 40, 5811–5816. https://doi.org/10.1021/es0607741

Montiel-León, J.M., Munoz, G., Vo Duy, S., Do, D.T., Vaudreuil, M.-A., Goeury, K., Guillemette, F., Amyot, M., Sauvé, S., 2019. Widespread occurrence and spatial distribution of glyphosate, atrazine, and neonicotinoids pesticides in the St. Lawrence and tributary rivers. Environmental Pollution 250, 29–39. https://doi.org/10.1016/j.envpol.2019.03.125

614 Moreno, A.I., Arnáiz, N., Font, R., Carratalá, A., 2014. Chemical characterization of emissions
615 from a municipal solid waste treatment plant. Waste Management 34, 2393–2399.
616 https://doi.org/10.1016/j.wasman.2014.07.008
617 Nguyen, P.Y., Carvalho, G., Reis, A.C., Nunes, O.C., Reis, M.A.M., Oehmen, A., 2017. Impact
618 of biogenic substrates on sulfamethoxazole biodegradation kinetics by Achromobacter
619 denitrificans strain PR1. Biodegradation 28, 205–217. https://doi.org/10.1007/s10532-
620 017-9789-6
621 Nuel, M., Laurent, J., Bois, P., Heintz, D., Mosé, R., Wanko, A., 2017. Seasonal and ageing
622 effects on SFTW hydrodynamics study by full-scale tracer experiments and dynamic time
623 warping algorithms. Chemical Engineering Journal 321, 86–96.
624 https://doi.org/10.1016/j.cej.2017.03.013
625 Nuel, M., Laurent, J., Bois, P., Heintz, D., Wanko, A., 2018. Seasonal and ageing effect on the
626 behaviour of 86 drugs in a full-scale surface treatment wetland: Removal efficiencies and
627 distribution in plants and sediments. Science of The Total Environment 615, 1099–1109.
628 https://doi.org/10.1016/j.scitotenv.2017.10.061
629 Ouedraogo, F.R., Zhang, J., Cornejo, P.K., Zhang, Q., Mihelcic, J.R., Tejada-Martinez, A.E.,
630 2016. Impact of sludge layer geometry on the hydraulic performance of a waste
631 stabilization pond. Water Research 99, 253–262.
632 https://doi.org/10.1016/j.watres.2016.05.011
633 Pelander, A., Tyrkkö, E., Ojanperä, I., 2009. *In silico* methods for predicting metabolism and
634 mass fragmentation applied to quetiapine in liquid chromatography/time-of-flight mass
635 spectrometry urine drug screening. Rapid Commun. Mass Spectrom. 23, 506–514.
636 https://doi.org/10.1002/rcm.3901
637 Petrie, B., Barden, R., Kasprzyk-Hordern, B., 2015. A review on emerging contaminants in
638 wastewaters and the environment: Current knowledge, understudied areas and
639 recommendations for future monitoring. Water Research 72, 3–27.
640 https://doi.org/10.1016/j.watres.2014.08.053
641 Phillips, P.J., Chalmers, A.T., Gray, J.L., Kolpin, D.W., Foreman, W.T., Wall, G.R., 2012.
642 Combined Sewer Overflows: An Environmental Source of Hormones and Wastewater
643 Micropollutants. Environmental Science & Technology 46, 5336–5343.
644 https://doi.org/10.1021/es3001294
645 Rožman, M., Acuña, V., Petrović, M., 2018. Effects of chronic pollution and water flow
646 intermittency on stream biofilms biodegradation capacity. Environmental Pollution 233,
647 1131–1137. https://doi.org/10.1016/j.envpol.2017.10.019
648 Rühmland, S., Wick, A., Ternes, T.A., Barjenbruch, M., 2015. Fate of pharmaceuticals in a
649 subsurface flow constructed wetland and two ponds. Ecological Engineering 80, 125–
650 139. https://doi.org/10.1016/j.ecoleng.2015.01.036
651 Schymanski, E.L., Singer, H.P., Slobodnik, J., Ipolyi, I.M., Oswald, P., Krauss, M., Schulze, T.,
652 Haglund, P., Letzel, T., Grosse, S., 2015. Non-target screening with high-resolution mass
653 spectrometry: critical review using a collaborative trial on water analysis. Analytical and
654 bioanalytical chemistry 407, 6237–6255.
655 Siegrist, H., Krebs, P., Bühler, R., Purtschert, I., Rock, C., Rufer, R., 1995. Denitrification in
656 secondary clarifiers. Water Science and Technology, Modelling and Control of Activated
657 Sludge Processes 31, 205–214. https://doi.org/10.1016/0273-1223(95)00193-Q
658 Tiwari, B., Sellamuthu, B., Ouarda, Y., Drogui, P., Tyagi, R.D., Buelna, G., 2017. Review on fate
659 and mechanism of removal of pharmaceutical pollutants from wastewater using
660 biological approach. Bioresource Technology 224, 1–12.
661 https://doi.org/10.1016/j.biortech.2016.11.042

Tong, Y., Wang, M., Peñuelas, J., Liu, X., Paerl, H.W., Elser, J.J., Sardans, J., Couture, R.-M., Larssen, T., Hu, H., Dong, X., He, W., Zhang, W., Wang, X., Zhang, Y., Liu, Y., Zeng, S., Kong, X., Janssen, A.B.G., Lin, Y., 2020. Improvement in municipal wastewater treatment alters lake nitrogen to phosphorus ratios in populated regions. Proc Natl Acad Sci USA 117, 11566–11572. https://doi.org/10.1073/pnas.1920759117

Verlicchi, P., Al Aukidy, M., Zambello, E., 2012. Occurrence of pharmaceutical compounds in urban wastewater: Removal, mass load and environmental risk after a secondary treatment—A review. Science of The Total Environment 429, 123–155. https://doi.org/10.1016/j.scitotenv.2012.04.028

Versteeg, H.K., Malalasekera, W., 2007. An introduction to computational fluid dynamics: the finite volume method, 2nd ed. ed. Pearson Education Ltd, Harlow, England ; New York.

Villette, C., Maurer, L., Delecolle, J., Zumsteg, J., Erhardt, M., Heintz, D., 2019. In situ localization of micropollutants and associated stress response in Populus nigra leaves. Environment International 126, 523–532. https://doi.org/10.1016/j.envint.2019.02.066

Villette, Claire, Maurer, L., Wanko, A., Heintz, D., 2019. Xenobiotics metabolization in Salix alba leaves uncovered by mass spectrometry imaging. Metabolomics 15, 122. https://doi.org/10.1007/s11306-019-1572-8

Vymazal, J., Dvořáková Březinová, T., Koželuh, M., Kule, L., 2017. Occurrence and removal of pharmaceuticals in four full-scale constructed wetlands in the Czech Republic – the first year of monitoring. Ecological Engineering 98, 354–364. https://doi.org/10.1016/j.ecoleng.2016.08.010

Wang, X., McCarty, P.L., Liu, J., Ren, N.-Q., Lee, D.-J., Yu, H.-Q., Qian, Y., Qu, J., 2015. Probabilistic evaluation of integrating resource recovery into wastewater treatment to improve environmental sustainability. PNAS 112, 1630–1635. https://doi.org/10.1073/pnas.1410715112

Yin, L., Wang, B., Yuan, H., Deng, S., Huang, J., Wang, Y., Yu, G., 2017. Pay special attention to the transformation products of PPCPs in environment. Emerging Contaminants 3, 69–75. https://doi.org/10.1016/j.emcon.2017.04.001

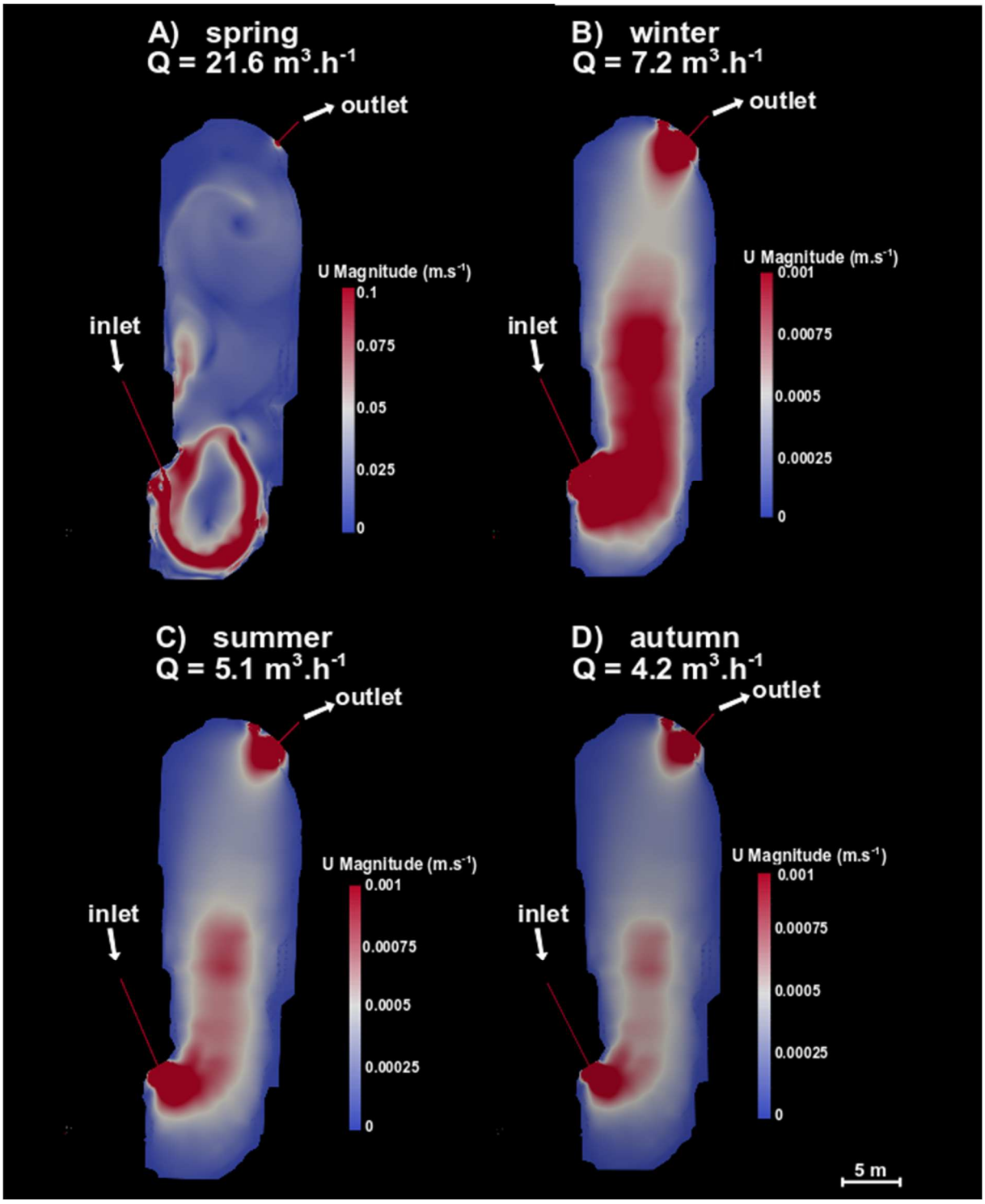

Figure 1. SFTW water flow in the different inlet flow rate conditions observed for each season. The water flow was simulated using the different conditions measured at the study site. The higher water flow monitored was approximately 21.6 $m^3.h^{-1}$ and was simulated in case A (spring). The conditions the most representative of average flow rate were observed in cases B (winter with 7.2 $m^3.h^{-1}$), C (summer with 5.1 $m^3.h^{-1}$), and D (autumn with 4.2 $m^3.h^{-1}$).

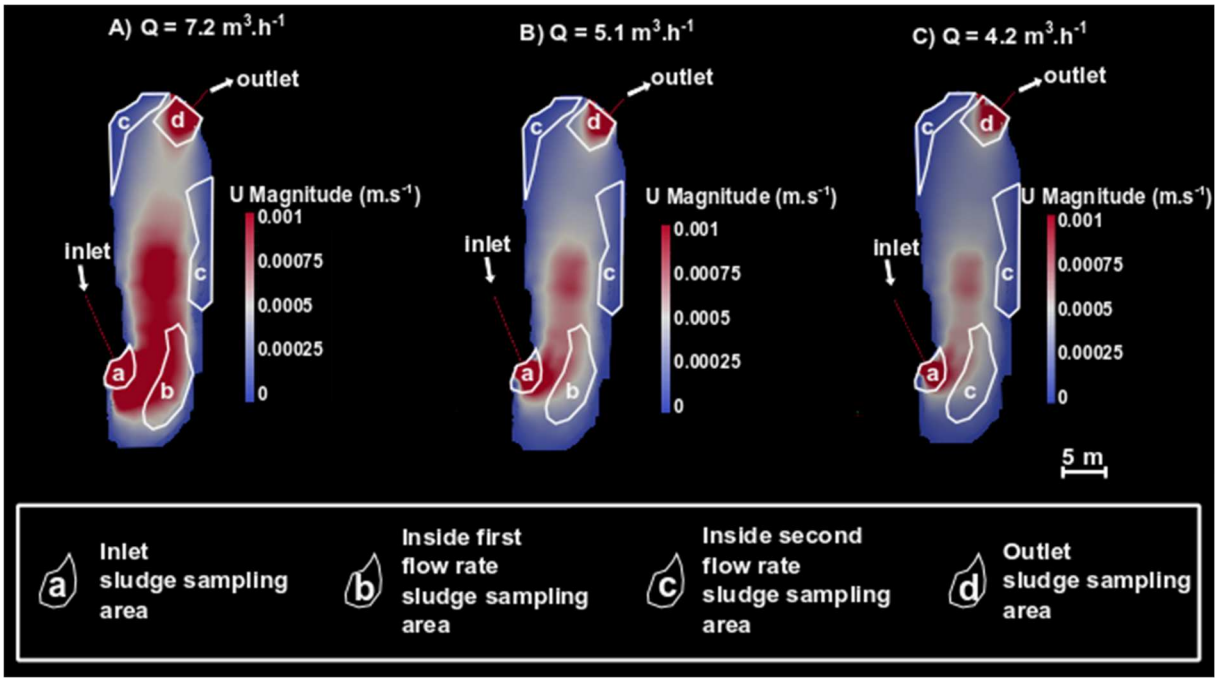

Figure 2. Water flow areas defining the sludge sampling strategy in the SFTW. Four areas based on similar water flow behaviour were selected to collect sludge. The sludge areas were chosen to represent faster and slower water flow areas inside and at the system limits. Thus sludge was sampled at inlet and outlet areas (a and d, respectively), in relatively lower flow areas (area c), and relatively higher flow areas (area b) inside the SFTW. A) Sampling strategy applied with an inlet flow rate of 7.2 $m^3.h^{-1}$. B) Sampling strategy applied with an inlet flow rate of 5.1 $m^3.h^{-1}$. C) Sampling strategy applied with an inlet flow rate of 4.2 $m^3.h^{-1}$. The spring simulation was not considered, as it was not representative of the average conditions.

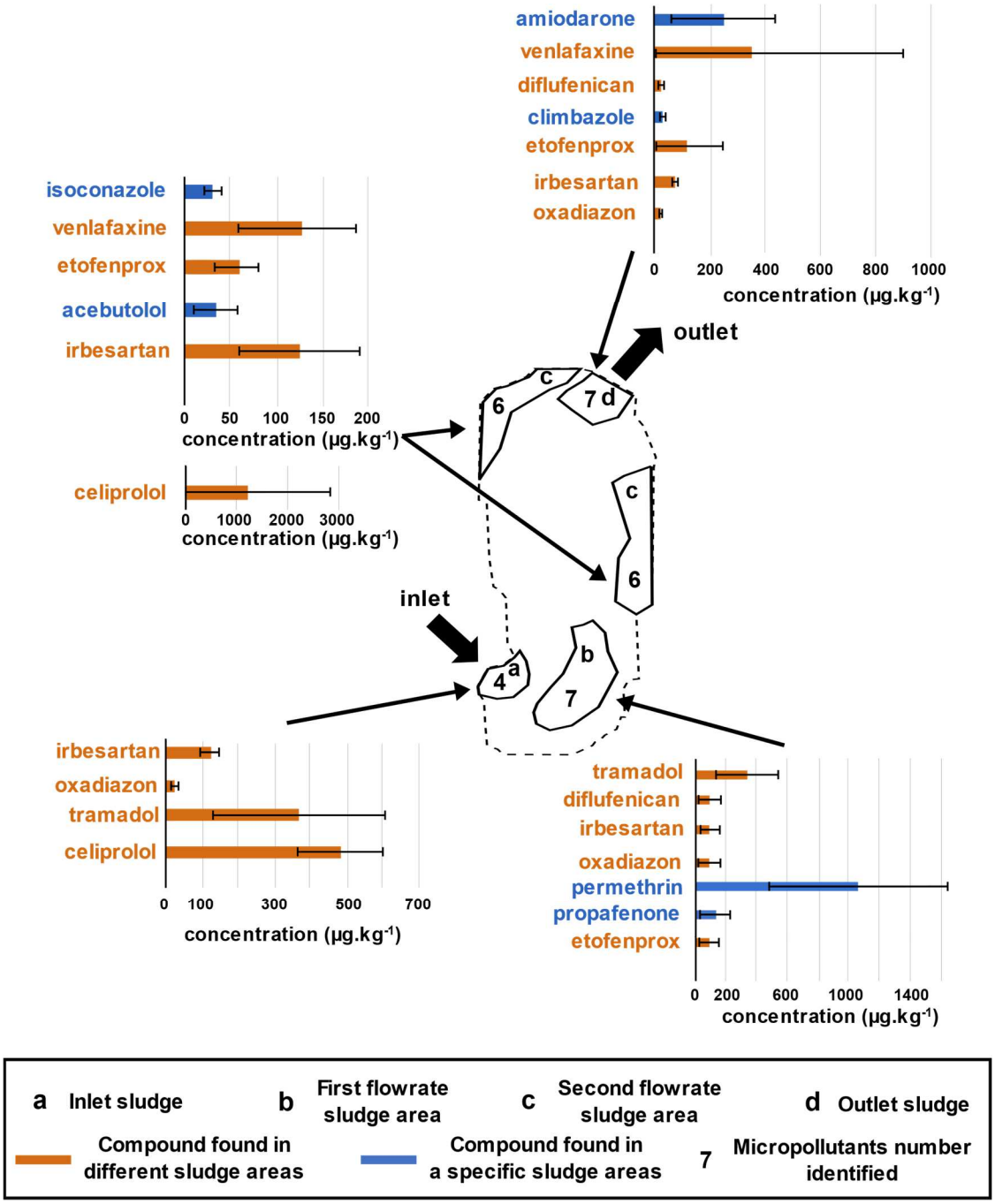

Figure 3. Distribution and quantification of micropollutants found for all seasons in the different flow rate areas of the SFTW. Compounds quantified were found in triplicates in each season. The concentration displayed shows the average concentration of all the samples; the standard deviation shows the concentration variability throughout the seasons. Compounds found in different sludge areas (orange) were distinguished from those found specifically in a single area (blue).

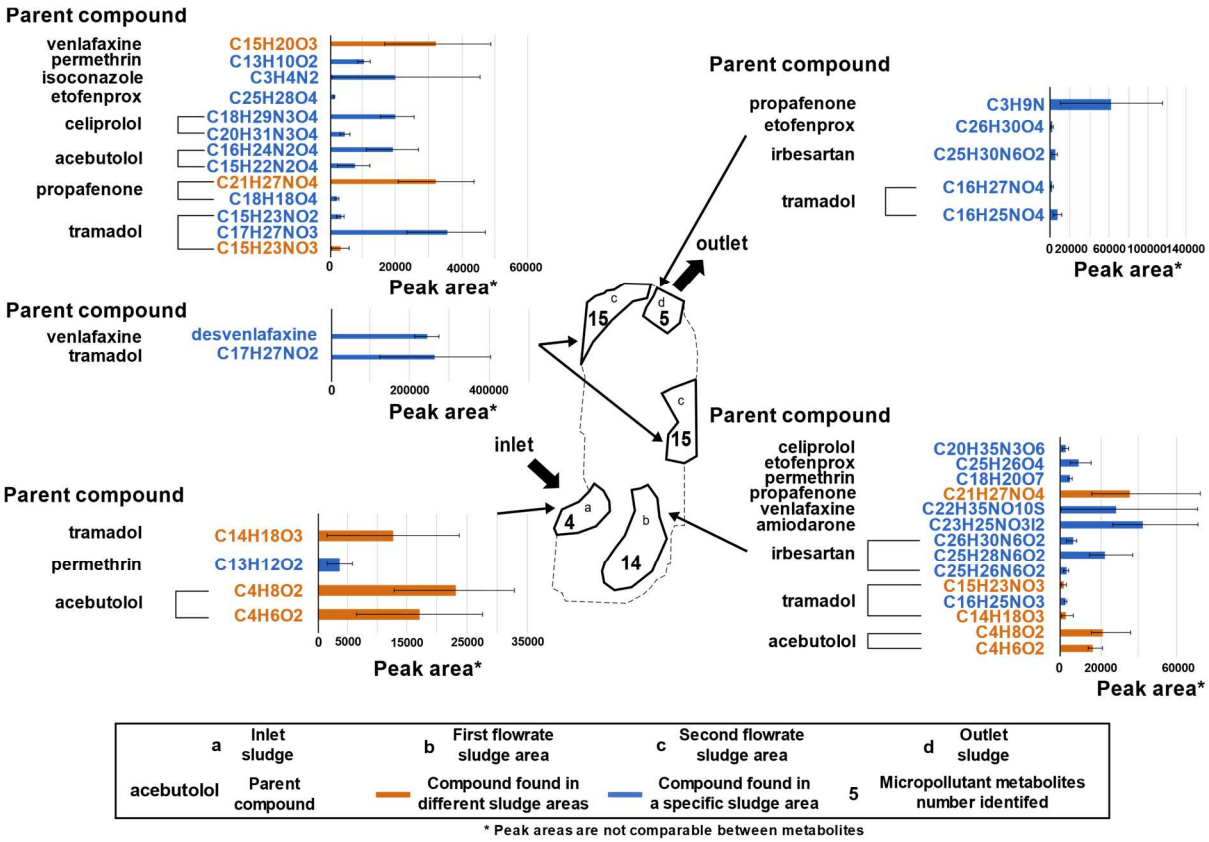

Figure 4. Distribution and intensity of micropollutants metabolites (catabolites and conjugated) found in each season in the different flow rate areas of the SFTW. The intensity displayed shows the average intensity of all the samples, and the standard deviation shows the intensity variability throughout the seasons. All the samples were analysed in triplicates for each season, and the standard deviation represents the intensity variation found through the seasons. Metabolites found in different sludge areas (orange) were distinguished from those found specifically in a single area (blue).

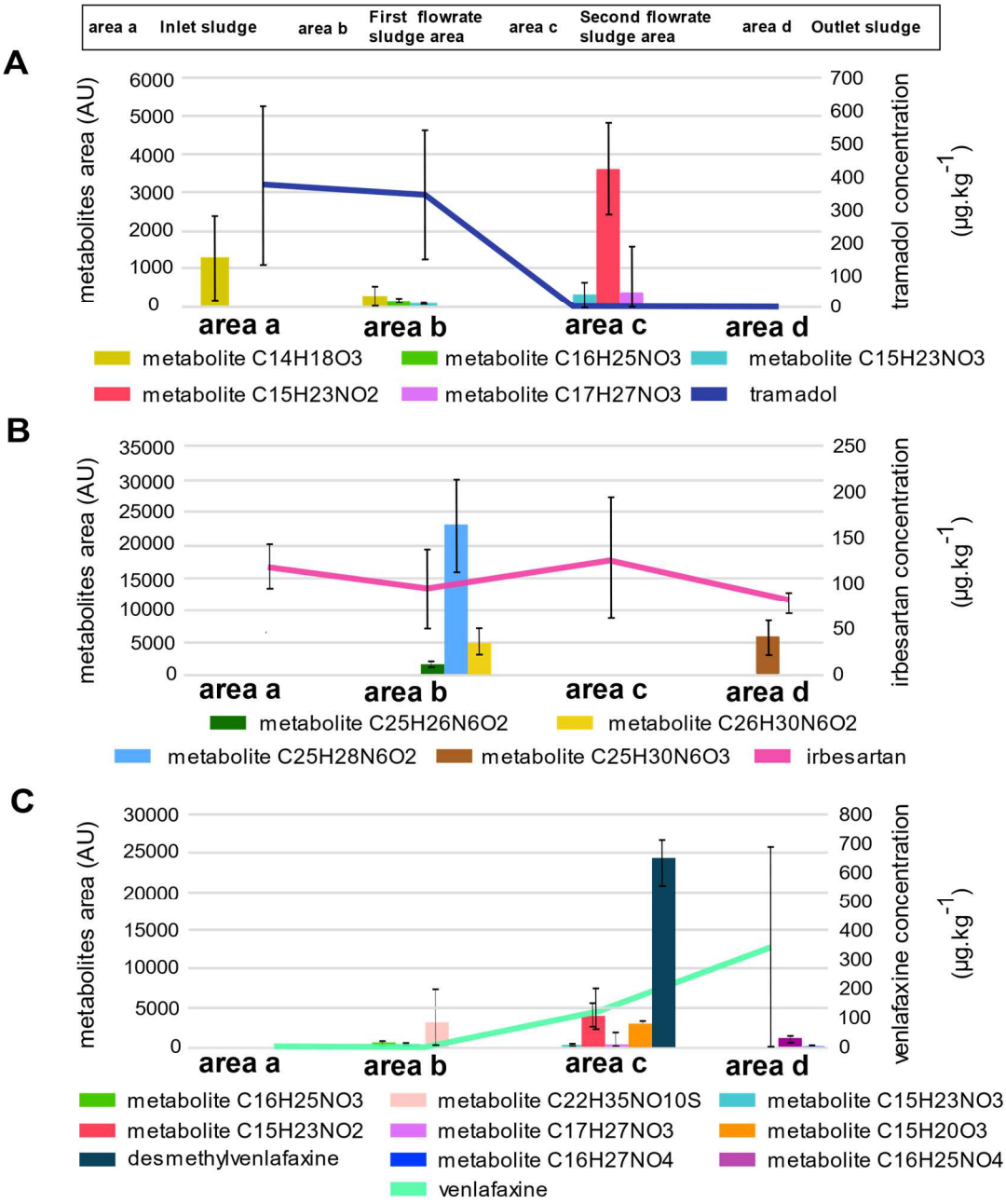

Figure 5. Distribution of tramadol, irbesartan, venlafaxine, and their metabolites in the different flow rate areas of the SFTW. A) Tramadol and its metabolites found in the different areas. B) Irbesartan and its metabolites found in the different areas. C) Venlafaxine and its metabolites found in the different areas. The concentration of parent compounds, found at least in two areas, is not correlated with the water flow areas. The metabolites of these compounds were primarily (higher intensity and diversity) found in the lower areas (b and c). All analyses were performed in triplicates for each season, and the standard deviation represents the concentration/intensity variation found through the seasons.

Micropollutants & metabolites analysis